Japanese Journal of Applied Physics
Vol. 46, No. 11, 2007, pp. 7356–7358

Brief Communication

The Impact of Fabrication Errors on a Flat-Top Grating-Based Planar Waveguide Demultiplexer

Chun-Ting LIN*, Yang-Tung HUANG[1], and Jung-Yaw HUANG

Department of Photonics and Institute of Electro-Optical Engineering, National Chiao Tung University, Hsinchu 30010, Taiwan
[1]*Department of Electronics Engineering and Institute of Electronics, National Chiao Tung University, Hsinchu 30010, Taiwan*

(Received May 14, 2007; accepted August 8, 2007; published online November 6, 2007)

The spectral performance of a demultiplexer is significantly affected by the phase and amplitude errors due to fabrication errors. We estimate the impact of fabrication errors on a flat-top grating-based planar waveguide demultiplexer using a design example. Simulation results show that the photomask resolution resulting in a phase error should be lower than 40 nm when a crosstalk criterion of −30 dB is given. The impact of amplitude errors is not distinct until the reduced amount of the facet width is greater than 0.5 µm and the grating side-wall angle offset from the vertical is larger than 1°.
[DOI: 10.1143/JJAP.46.7356]

KEYWORDS: planar waveguide, etched diffraction grating, flat-top, crosstalk, insertion loss, phase and amplitude errors, wavelength-division multiplexing (WDM)

Recently, great progress has been made toward developing demultiplexers with low insertion loss, low crosstalk, high possibilities of mass production, and high spectral resolution for dense wavelength division multiplexing (DWDM) systems. Planar waveguide demultiplexers, such as arrayed waveguide gratings (AWGs) and planar waveguide concave (etched) gratings, attract recent interests due to superior dispersive characteristics. However, a conventional planar waveguide demultiplexer has a Gaussian-like spectral response and is temperature-sensitive. The design of a flat-top demultiplexer provides an efficient solution to solve the problem. In this paper, a design example of a flat-top demultiplexer based on a planar waveguide concave grating is used to quantitatively estimate the impact of fabrication errors on the crosstalk and insertion loss of a flat-top demultiplexer based on a planar waveguide concave grating.

Fabrication errors, which come from nonidealities during the fabrication process, result in random phase and amplitude errors in the analysis using the diffraction theory.[1–5] The phase errors mainly come from the deviations of the positions for the vertices of the grating facets due to discrete multiples of an address unit defined by the electron beam mask generation system.[4] The amplitude errors mainly come from the roundings of the grating corners[4] and the grating side-wall angle offset from the vertical.[5] In our analysis, these parameters caused by fabrication errors are all taken into consideration. A flat-top design of a planar waveguide concave grating based on the recursive definition of facet positions, which was first proposed by McGreer in 1996,[6] is achieved when the three-focal-point method is used.[7] Using the Kirchoff–Huygens' diffraction integral formula, the spectral response of one channel at the design wavelength λ_0 of 1550.12 nm can be obtained. According to the corresponding phase and amplitude errors, the spectral characteristics of the demultiplexer are analyzed.

A planar waveguide concave grating as a flat-top demultiplexer based on the recursive definition of facet positions[7] shown in Fig. 1 is investigated, and this recursive definition design can have free-aberration characteristics. The device design is based on a silica-on-silicon waveguide

*E-mail address: rhino.eo91g@nctu.edu.tw

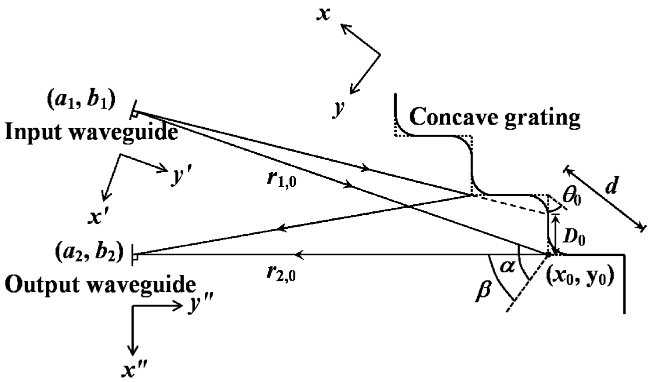

Fig. 1. Schematic figure of the light diffracted by the concave grating.

structure, which is composed of a lower 10-µm-thick SiO_2 cladding layer, a 6-µm-thick SiON core layer, and an upper 6-µm-thick SiO_2 cladding layer with the refractive indices of 1.450, 1.456, and 1.450 at the design wavelength of 1550.12 nm, respectively. By using the transfer-matrix method, the effective indices of the TE and TM modes are obtained as 1.453928 and 1.453917 with the propagation losses of 4.90×10^{-3} and 2.75×10^{-2} dB/cm, respectively.

The grating formed by etching a trench to the lower cladding layer is coated with aluminum at the back wall. Assuming no scattering loss at the grating facet, the reflection coefficient is assumed to be unity. The input and output waveguides are formed by a SiON core channel with a $6 \times 6\,\mu m^2$ cross-sectional area surrounded by the SiO_2 cladding layer. The spot sizes, w_{inwg} and w_{outwg}, of the fundamental mode for the input and output waveguides along the x'-axis and x''-axis, as shown in Fig. 1, are 4.08 µm. The Gaussian field[8] launched from the input waveguide is diffracted by the grating, refocused at the focal curve, and then guided into different output waveguides according to the corresponding wavelengths. $\alpha = 60°$ is the incident angle at the grating pole, $\beta = 57.12°$ is the mth-order diffraction angle of the design wavelength at the grating pole, $m = 16$ is the diffraction order, $d = 10\,\mu m$ is the grating period along the grating chord, and $\lambda_0 = 1550.12$ nm is the design wavelength. The half angle σ ($= \lambda_0/\pi n_{eff} w_{inwg}$) for the Gaussian beam divergence at $1/e$ amplitude is obtained as 4.77° for the TE mode. The

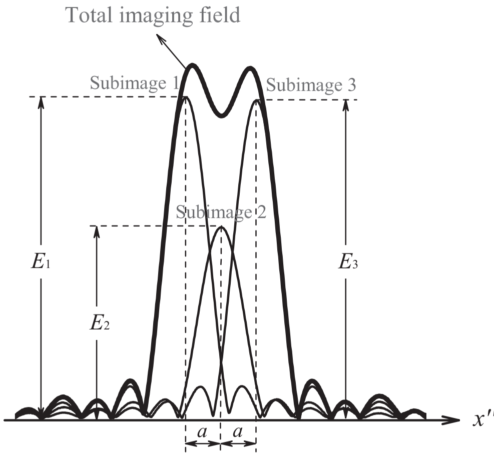

Fig. 2. Field distribution of three subimages at the ending facet for the output waveguide.

distances from the end of the input waveguide and the end of the output waveguide of the design wavelength to the grating pole are $r_{1,0} = 35000$ and $r_{2,0} = 35000\,\mu\text{m}$, respectively. The number of grating periods is $N = 1164$ and the effective radius of the grating $R = 67011\,\mu\text{m}$.

To obtain a flattened spectral response, the grating is composed of three interleaved subgratings[7)] and each forms a subimage with a different focal point lying on the cross-sectional line of the ending facet for the output waveguide, as shown in Fig. 2, where E_1, E_2, and E_3 denote the peak amplitudes of three subimages and $2a$ denotes the separation between the two outmost subimages (subimage 1 and subimage 3). To obtain a symmetric spectral response, E_1 and E_3 are chosen to be identical and the ratio of the peak amplitudes for the subimages is approximately equal to the ratio of the facet numbers for the corresponding subgratings. Because three subgratings are interleaved, the spot size w_{image} of each subimage along the x''-axis is identical and is obtained as $4.87\,\mu\text{m}$. Simulation results show that when the ratio E_2/E_1 is chosen to be 1, the optimal half-separation a between the two outmost subimages is obtained as $1.74 w_{\text{outwg}}$ with a minimum ripple. The ripple is defined as the maximum difference among three extremum points within the -3-dB passband of one channel. The -3-dB passband width is 30.87 GHz with a crosstalk of -40.62 dB. The insertion loss in our case is 4.64 dB, where 2.43 dB comes from the excess loss, obtained from the overlap integral of the imaging field with the output waveguide mode field, and 2.21 dB comes from the undesired-order loss, resulting from the diffraction of light into undesired adjacent orders.

The phase errors, which are mainly caused by the deviations of the positions for the vertices of the grating facets, lead to the deterioration in the spectral response. The standard deviation σ_{p} of the position errors, i.e., the resolution of the photomask, is defined as

$$\sigma_{\text{p}} = \sqrt{\sigma_{\text{p}x}^2 + \sigma_{\text{p}y}^2} = \sqrt{\frac{1}{N-1}\sum_i (\Delta x_i^2 + \Delta y_i^2)}, \qquad (1)$$

where Δx_i and Δy_i are the deviations of the positions for the vertices of the ith grating facet along the x-axis and y-axis, respectively. Δx_i and Δy_i are randomly generated by a computer and they are normalized with an assigned value σ_{p}. The crosstalks of the central channel versus various standard deviations σ_{p} for 20 samples are shown in Fig. 3 when the channel spacing $\Delta\lambda_{\text{channel}}$ is 0.4 nm (50 GHz). It shows that when σ_{p} increases from 0 to 100 nm, the mean value of the crosstalks increases from -40.62 to -25.86 dB. It also shows that when the crosstalk criteria of -30 dB in our case is given, a photomask resolution lower than 40 nm is required. The phase errors are the main sources of the crosstalk. The corresponding -3-dB passband widths of the central channel for 20 samples are shown in Fig. 4. It shows that the fluctuation of the -3-dB passband width increases as the standard deviation σ_{p} of the position errors increases.

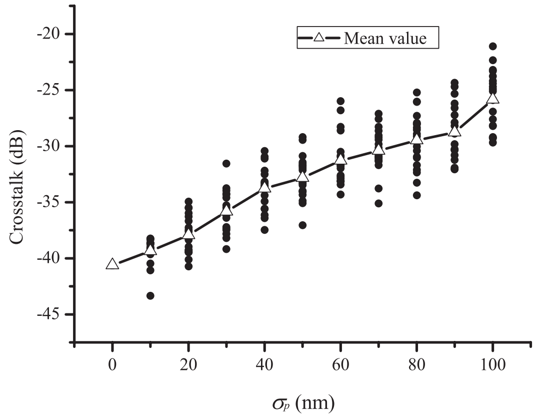

Fig. 3. Crosstalks of the central channel versus various standard deviations σ_{p} for 20 samples when the channel spacing $\Delta\lambda_{\text{channel}}$ is 0.4 nm (50 GHz).

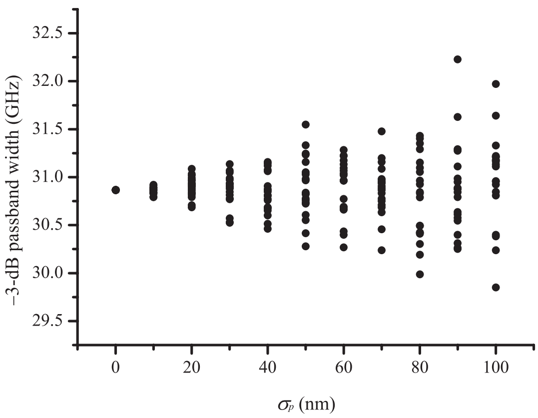

Fig. 4. -3-dB passband widths of the central channel versus various standard deviations σ_{p} for 20 samples when the channel spacing $\Delta\lambda_{\text{channel}}$ is 0.4 nm (50 GHz).

The corner roundings of the grating facets reduce the effective facet widths D_i, as shown in Fig. 1, and then increase the insertion loss when the light reflected from the rounding facets is lost. In our design, the facet widths D_i range from 5.00 to $5.12\,\mu\text{m}$. It is assumed that all grating facets have the same width reduction ΔD due to the corner roundings to evaluate the additional loss caused by the corner roundings and Fig. 5 shows the results. The additional loss increases as the width reduction ΔD increases as expected, and this additional loss is 0.92 dB when the width reduction ΔD is $0.5\,\mu\text{m}$. The other challenge of fabricating

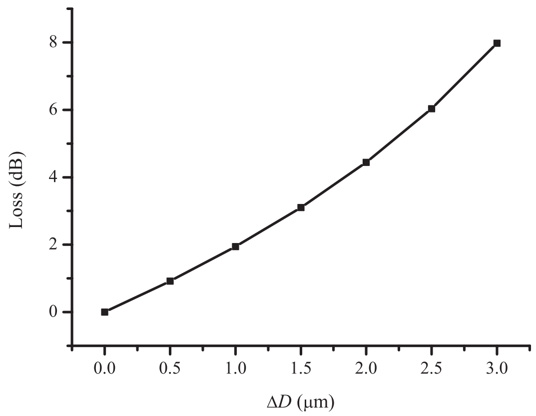

Fig. 5. Loss caused by the corner roundings of the grating facets.

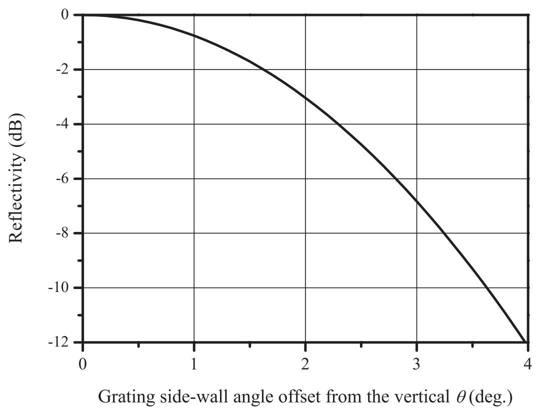

Fig. 6. Loss caused by the side-wall angle offset from the vertical.

the etched diffraction grating (EDG) is to achieve a nearly vertical grating side wall. The reflectance R affected by the side-wall angle offset from the vertical with a small tilt angle θ can be expressed as[9)]

$$R = 10 \log e^{-(2\theta/\theta_{\rm d})^2}, \tag{2}$$

$$\theta_{\rm d} = \frac{\lambda_0}{\pi n_{\rm eff}\omega_0}, \tag{3}$$

where $\omega_0 = 4.07\,\mu$m is the spot size of the slab waveguide mode along the z-axis. The simulation results, as shown in Fig. 6, predict that a side-wall angle offset of 1° from the vertical will lead to an additional loss of more than 0.76 dB. When the width reduction and grating side-wall angle offset are $0.5\,\mu$m and $\pm 1^\circ$, the additional losses are 0.92 and 0.76 dB, respectively, which contribute to an acceptable additional loss below 2 dB.

In this paper, the impact of fabrication errors relevant to the phase and amplitude errors on a flat-top planar waveguide demultiplexer is evaluated. Simulation results show that the phase errors caused by the deviations of the positions for the vertices of the grating facets are the main sources of the crosstalk, and the amplitude errors caused by the roundings of the grating corners and the grating side-wall angle offset from the vertical cause additional losses. When the standard deviation of the position errors increases from 0 to 100 nm, the mean value of the crosstalks for 20 samples increases from -40.62 to -25.86 dB. With a crosstalk criteria of -30 dB in our case, a photomask resolution lower than 40 nm is required. To achieve a flat-top planar waveguide demultiplexer with good performance, fabrication errors must be taken into consideration.

Acknowledgements

This work was supported in part by the National Science Council, Taiwan, R.O.C. under the contract NSC 95-2221-E-009-250.

1) C. D. Lee, W. Chen, Q. Wang, Y.-J. Chen, W. T. Beard, D. Stone, E. F. Smith, R. Mincher, and I. R. Stewart: J. Lightwave Technol. **19** (2001) 1726.
2) Y. Chu, X. Zheng, H. Zhang, X. Liu, and Y. Guo: IEEE J. Sel. Top. Quantum Electron. **8** (2002) 1122.
3) H. Wen, D. Pang, and Z. Qiang: Opt. Commun. **236** (2004) 1.
4) R. J. Deri, J. S. Kallman, and S. P. Dijaili: IEEE Photonics Technol. Lett. **6** (1994) 242.
5) S. Janz, A. Balakrishnan, S. Charbonneau, P. Cheben, M. Cloutier, A. Delâge, K. Dossou, L. Erickson, M. Gao, P. A. Krug, B. Lamontagne, M. Packirisamy, M. Pearson, and D.-X. Xu: IEEE Photonics Technol. Lett. **16** (2004) 503.
6) K. A. McGreer: Appl. Opt. **35** (1996) 5904.
7) Z. Shi and S. He: IEEE J. Sel. Top. Quantum Electron. **8** (2002) 1179.
8) K. A. McGreer: IEEE Photonics Technol. Lett. **7** (1995) 324.
9) W. van Etten and J. van der Plaats: *Fundamentals of Optical Fiber Communications* (Prentice Hall, New York, 1991) p. 253.